Supplementary Information for

Seamless interconnections of sp^2-bonded carbon nanostructures via crystallization of a bridging amorphous carbon joint

*Longze Zhao[#], Yong Cheng[#], Qiaobao Zhang, and Ming-Sheng Wang**

Department of Materials Science and Engineering, College of Materials, and Pen-Tung Sah Institute of Micro-Nano Science and Technology, Xiamen University, Xiamen, Fujian 361005, China.

*Corresponding author. E-mail: mswang@xmu.edu.cn

[#]L. Zhao and Y. Cheng contributed equally to this work.

Supplementary Figures

Figure S1-S8

Supplementary Movies

Movie S1

1. The improvement of the structural perfection of the joined nanotube during a prolonged annealing process

After the two nanotubes were joined by the e-beam induced deposition of a-C (Figure S1a), a prolonged annealing process was carried out. During the process, the applied current was increased carefully to avoid the breakdown of the CNT junction. At the beginning of the annealing process, there existed many distinct kink structures, and the junction was slightly bent (Figure S1b). As the annealing process continued, the kinks largely disappeared and the bending junction evolved into a straight nanotube (Figure S1b-g). The inner closed structures changed a lot in morphology and some nano onions disappeared from the junction region, while the outer three shells across the junction maintained their structural integrity and became more regular.

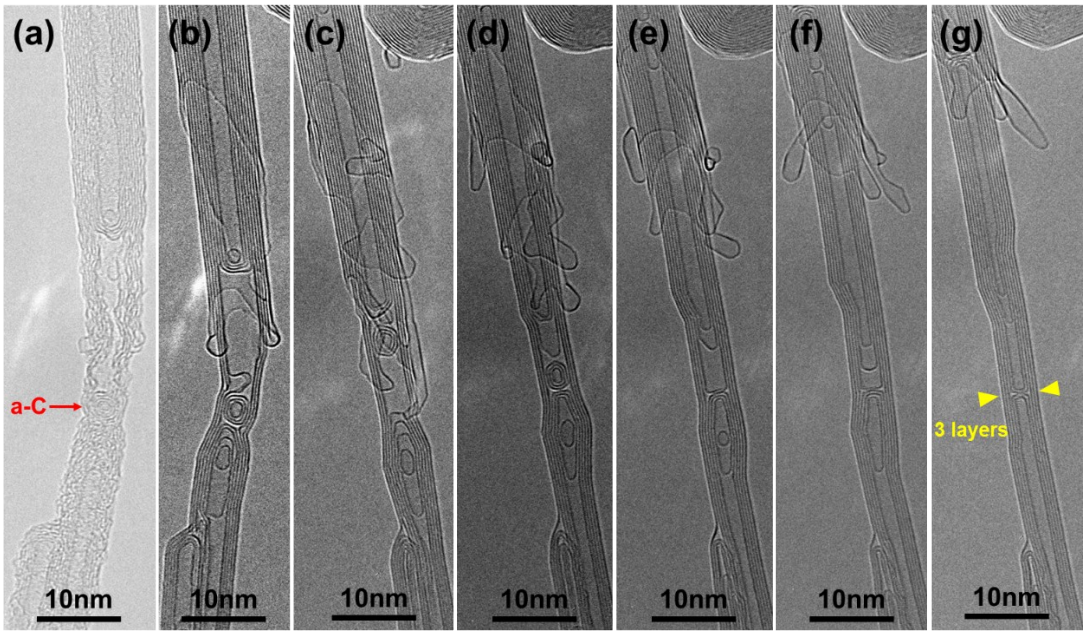

Figure S1. (a) The joined carbon heterostructure with the central a-C as a joint. (b-g) Structural evolution of the junction during a prolonged annealing process.

2. The repairing of two nanotube segments with a regular open end

Figure S2 shows the repairing process of a nanotube that broke into two segments with a regular open end. The two nanotube segments were connected through crystallization of the a-C joint as described in the main text. The HRTEM image in Figure S2e demonstrates the as-formed outer continuous layers across the junction and the closed nanostructures encapsulated inside the channel.

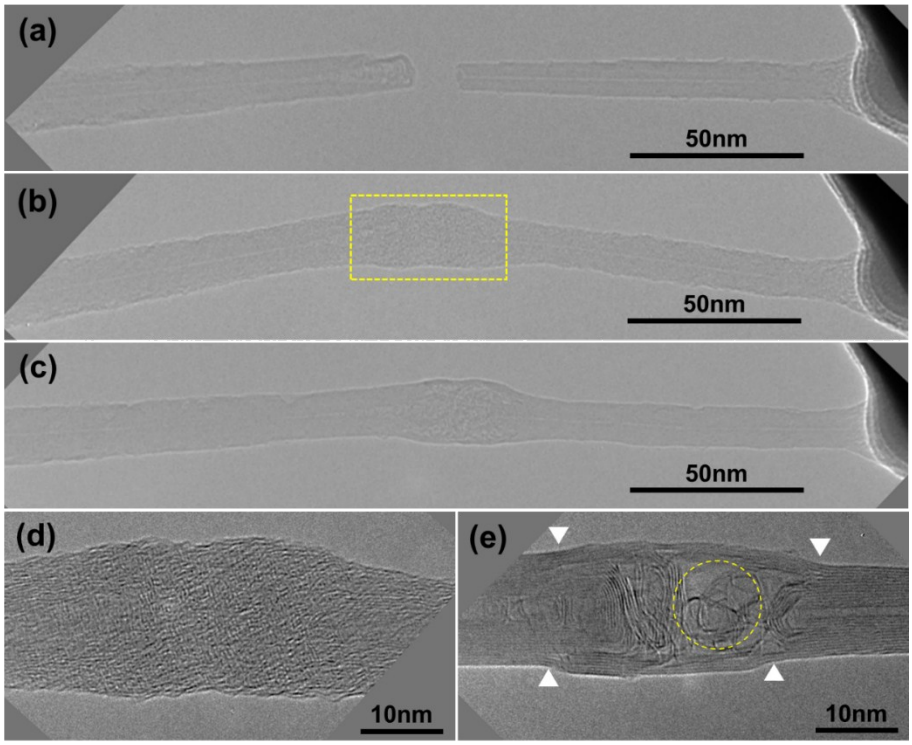

Figure S2. TEM images showing the repairing process of a broken nanotube (a) The nanotube was cut into two segments after electric breakdown. (b) EBID of a-C at the gap between the two tube segments. (c) The junction after a thermal annealing process induced by passing a large current through it. (d) HRTEM image of the a-C joint in the boxed region in (b). (e) HRTEM image showing the junction after annealing. The white arrowheads indicate the tubular graphene layers at the junction region that seamlessly connect the two tube segments, and the yellow circle indicates the closed carbon nanostructures inside the junction.

3. The connection between different tube shells derived from the same MWNT

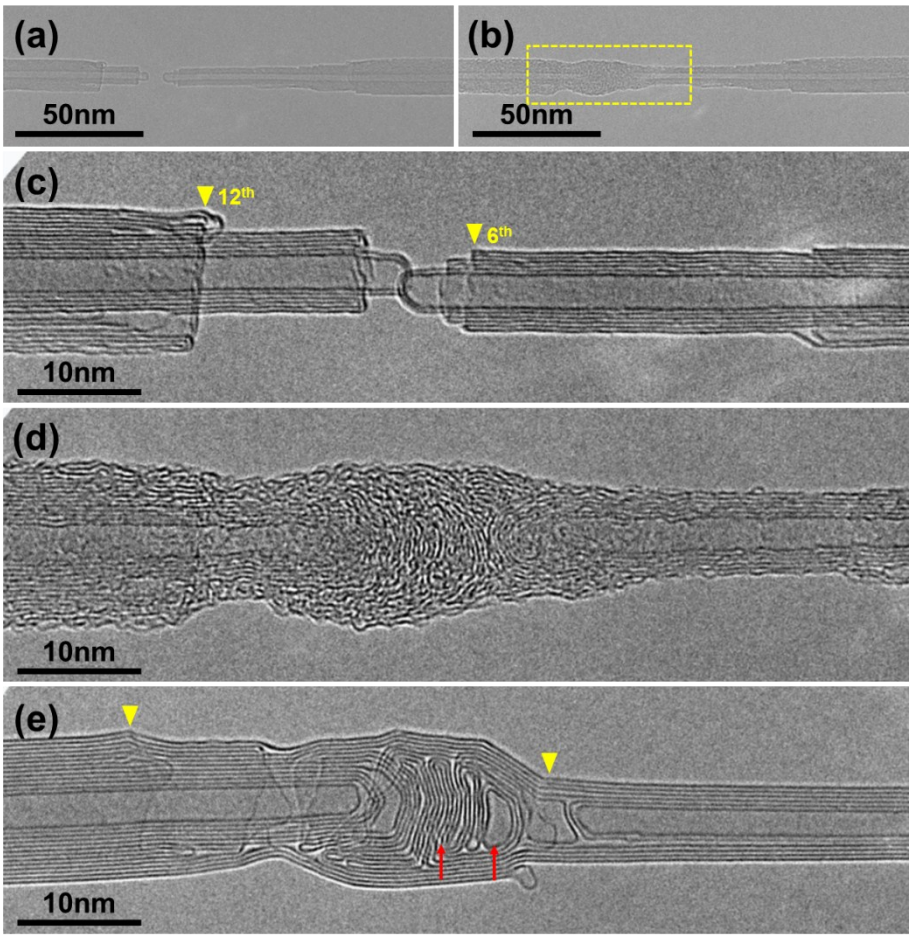

Figure S3. TEM images showing the repairing process of a broken MWNT. (a) The nanotube broke into two segments after electric breakdown. (b) EBID of a-C at the gap between the two tube segments. (c) HRTEM image showing the end structures of these two segments. The arrowheads indicate the outermost shells. (d) HRTEM image showing the junction after EBID of a-C, in the region indicated in (b). (e) HRTEM image of the junction after annealing. The yellow arrowheads indicate the outermost shells of these two segments that were joined to form a continuous layer, and the red arrows indicate the closed nanostructures inside the junction.

Figure S3 shows another case for MWNT repairing. After electrical breakdown, two step-like CNT segments were formed (Figure S3a,c). The outermost shells to be connected for these two nanotube segments are the 12^{th} and 6^{th} layers respectively, as indicated by the arrowheads in Figure S3c. The a-C was then deposited at the junction

region, and both outermost shells of the two tube segments were coated by a layer of a-C (Figure S3b,d). After annealing, both outermost shells, i.e. the 12^{th} (for the left segment) and 6^{th} (for the right segment) layers of the pristine MWNT, were connected with each other, as indicated by the yellow arrowheads in Figure S3e. The a-C in the interior crystalized into nano-onion structures, exhibiting graphitic layers perpendicular to the tube axis, as indicated by the red arrows. Therefore, two different tube shells of the pristine MWNT were seamlessly joined during CNT repairing.

4. The seamless connection between thin and thick MWNTs

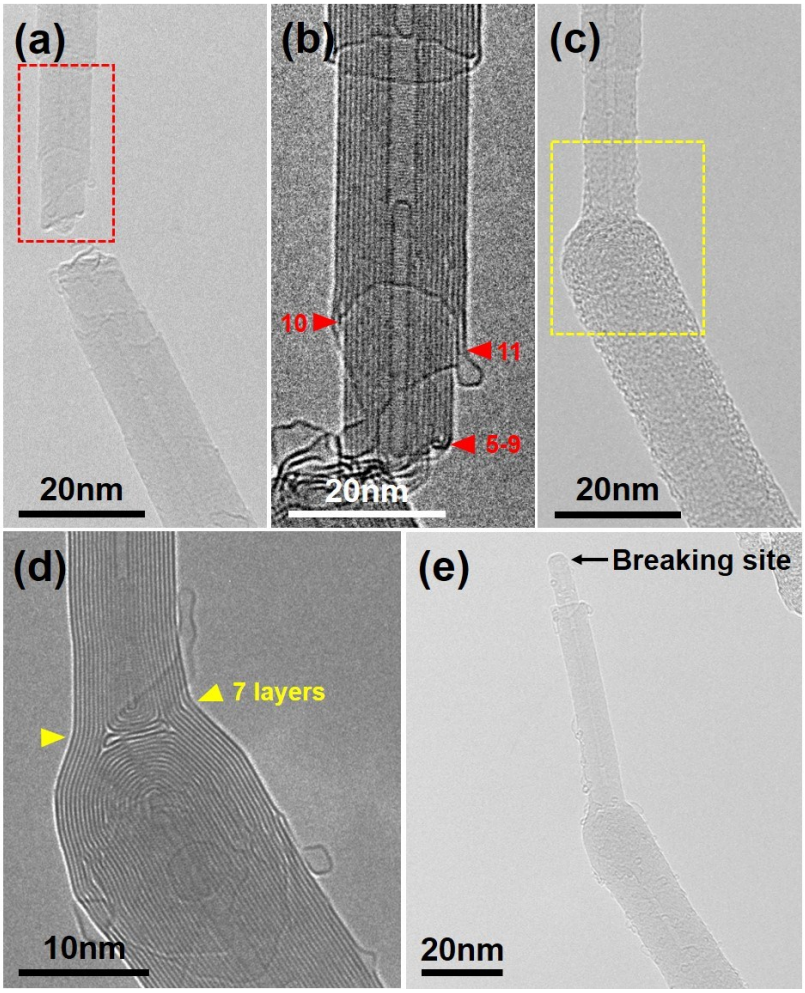

Figure S4. TEM images showing a typical case for seamless connection of thin and thick CNTs. (a) Two nanotubes that were brought close to form a gap between them. (b) HRTEM image showing the upper thinner nanotube. The red arrowheads indicate the open shells to be connected. (c) EBID of a-C at the gap between the two nanotubes. (d) HRTEM image showing the annealed junction in the indicated region in (c). (e) The junction after electrical breakdown. The arrow indicates the breaking site at the thinner nanotube section.

Figure S4 shows a more representitive case for CNT connection, where the two joined nanotubes were distinctly different in diameter and shell number (and chirality as well). In this case, there were 7 layers extending across the entire junction, which was constructed by two CNT segments with 11 and 19 shells respectively (Figure S4d).

The HRTEM images in Figure S4b and S4d reveal that the open-ended shells 5-11 of the upper tube segments (as indicated by the arrowheads in Figure S4b) were involved in the building of continuous layers across the junction. Finally, an electrical breakdown occurred at the thinner tube section at an increasing current, indicating the higher current carrying capacity of the junction than the thinner nanotube (Figure S4e).

5. Creation of a seamless right-angled junction

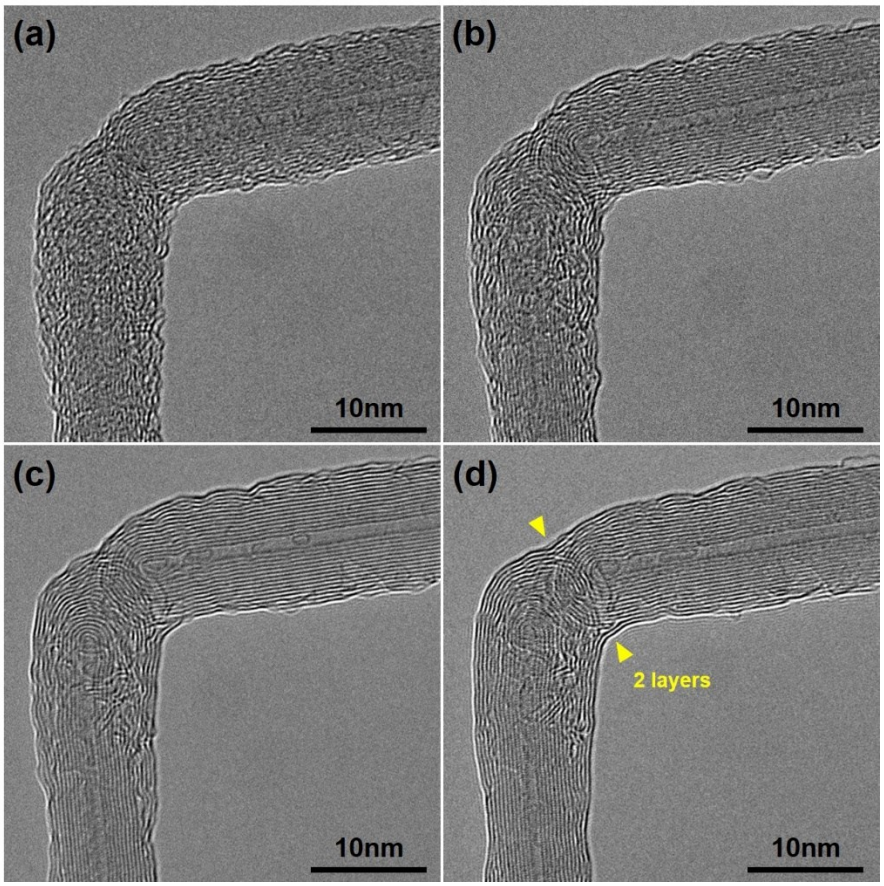

Figure S5. A series of HRTEM images showing the structural transformation of a right-angled junction during annealing. (a) The two nanotubes joined by the deposited a-C. (b, c) Structural evolution of the junction during annealing. (d) The final crystalized junction. The yellow arrowheads indicate the continuous graphitic layers cross the junction.

This joining technique can also be employed to construct the seamless CNT junctions with any desired connecting angle, e.g. a right angle. Figure S5 shows a joining process of two CNTs aligned perpendicular to each other. HRTEM images in Figure S5 display the structural evolution of the junction during its amorphous-crystalline transition. As indicated by the yellow arrowheads in Figure S5d, there existed at least two outer graphitic layers, curved but continuous, extending throughout the surface of the crystalized junction. We can also observe that the rest of the a-C has

transformed into two opposite CNT caps (overlapped with each other in the projection TEM image due to the slight vertical drift of the W tip during the a-C deposition) encapsulated in the outer shells after annealing.

6. The mechanical properties simulations of the CNT junctions

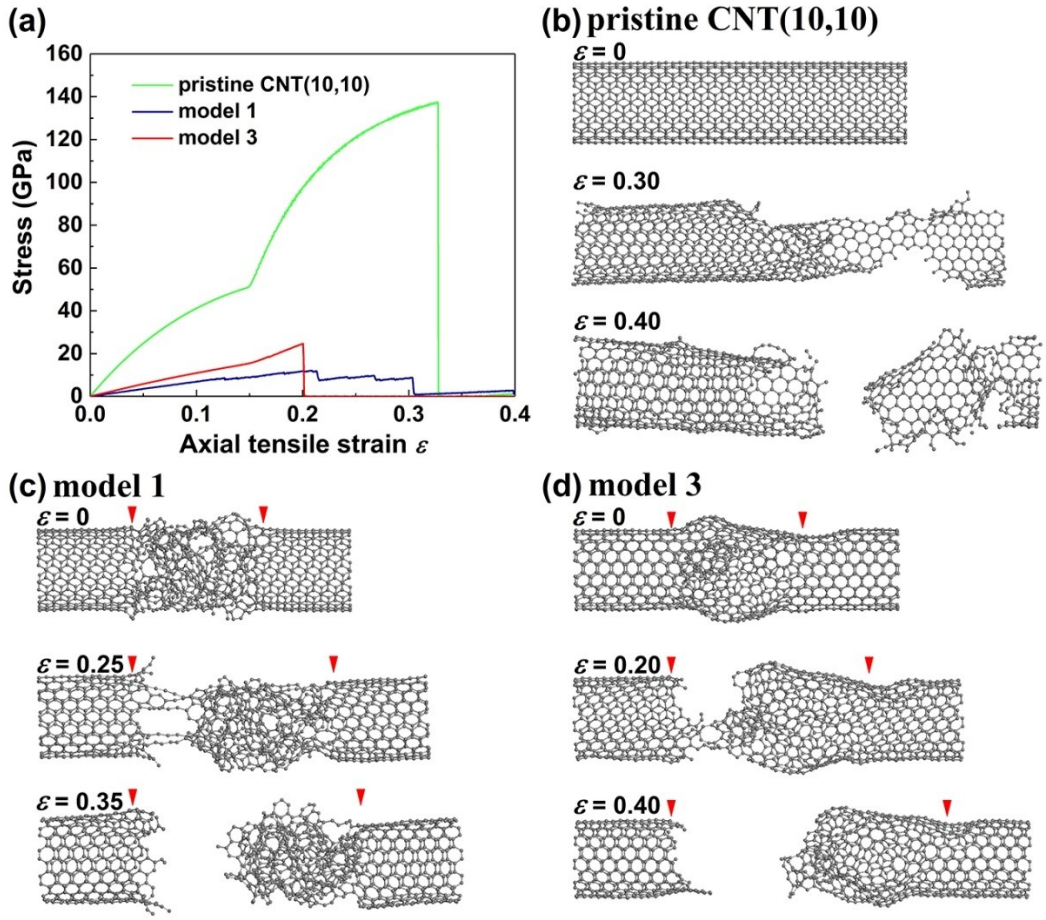

Figure S6. Theoretical simulation of mechanical properties of CNT junctions and pristine CNT (10, 10). (a) Stress–strain curves of pristine CNT (10, 10), junction models 1 and 3 under axial tensile loading. (b-d) The brittle fracture processes of pristine CNT (10, 10), models 1 and 3 respectively.

Figure S6 shows the mechanical properties evaluation of the CNT junctions (Models 1 and 3 in Figure 4 in the main text), as well as the results of pristine CNT (10, 10) for comparison, by using molecular dynamics simulations. The results show that the tensile strengths of junctions 1 and 3 are 12 and 24 GPa respectively, indicating a twofold increase in mechanical toughness caused by crystallization of a-C. Obviously, both values are much lower than that of pristine (10, 10) SWNT, i.e. 137 GPa (close to other theoretical results of ~140 GPa),[1] which can certainly be attributed to the

existence of structural defects within the junction. Figure S6b-S6c present the detailed brittle fracture processes of pristine CNT (10, 10), junctions 1 and 3 respectively. For the perfect pristine CNT (10, 10), the fracture occurs near the middle part of the tube. Instead, for the CNT junctions, bond breaking takes place more easily at the a-C/CNT interfaces due to the existence of defects.

7. CNT-graphene seamless interconnections

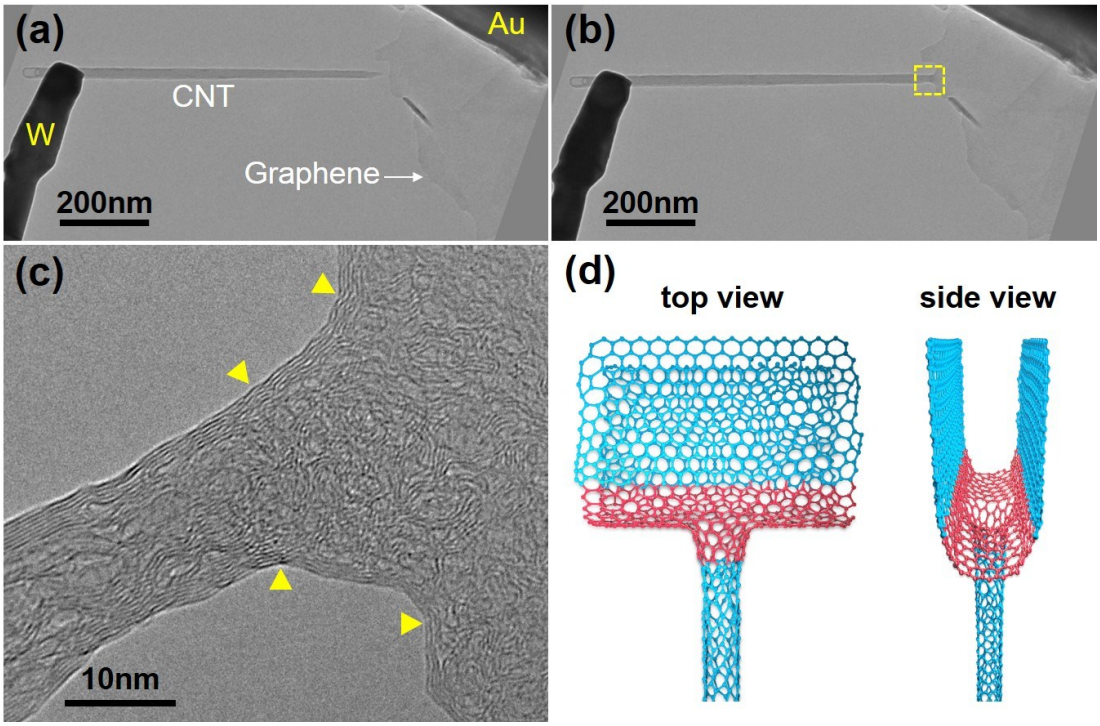

Figure S7. Seamless connection between CNT and graphene. (a) A nanotube attached on a W tip was brought close to a piece of graphene sheet to form a gap between them. (b) EBID of a-C at the gap between the nanotube and graphene sheet. (c) HRTEM image showing the junction region (the boxed region in (b) after annealing. The yellow arrowheads indicate the curved graphitic layers or closed graphene edges. (d) A simplified structural model showing the CNT-graphene connection via a coherent sp^2 carbon network.

We further extended this technique to the seamless connection between different sp^2 carbon allotropes, e.g. 1D nanotube and 2D graphene. A nanotube attached on a W tip obtained by electrical breakdown was moved close to a piece of graphene sheet, forming a gap between the tube end and the open graphene edge (Figure S7a). Then, a junction between these two carbon nanostructures was constructed through crystallization of the a-C joint as described above (Figure S7b). The annealing process caused a reduction in the overall resistance from 175.3 kΩ to 45.8 kΩ. HRTEM observations suggest that the outer surface of the a-C joint has transformed into

continuous graphitic layers, forming seamless connections between the graphene layers and CNT shells (Figure S7c). The dark fringe as indicated by the arrowheads in HRTEM images represent the curved shells or closed graphene edges. We thus proposed a simplified structural model in Figure S7d, illustrating how a nanotube and graphene sheet can be joined to form a coherent carbon network. Actually, in the previous in-situ TEM observation on graphene edge reconstructions by Joule heating, similar carbon nanostructures, i.e. two neighboring bilayer graphene interconnected by a SWNT, were occasionally found.[2] Differently, in the present work, we tried to build such CNT-graphene junctions in a controllable way. To the best of our knowledge, we present the first successful attempt in this regard.

8. In-situ tensile test of the CNT-graphene seamless junction

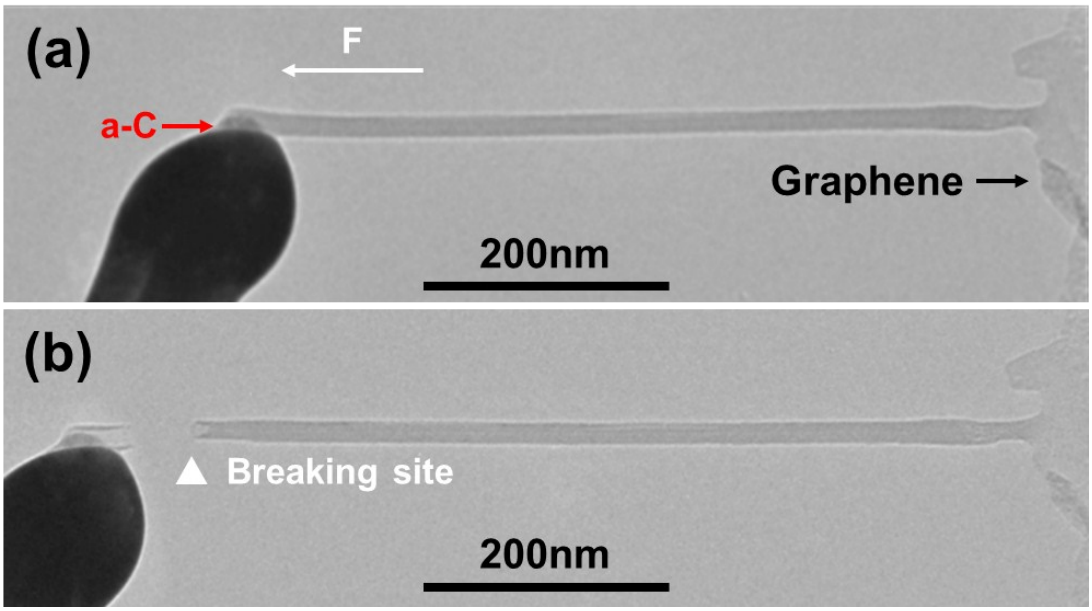

Figure S8. In-situ tensile test of the CNT-graphene junction. TEM images showing the junction before the tensile loading (a), and its breakage at the nanotube section (b).

To explore the mechanical property of the CNT-graphene junction as shown in Figure S7, an in-situ tensile test was conducted (Figure S8). The nanotube was welded firmly to the W tip by depositing a-C at the contact before the tensile test (Figure S8a). By retracting the W tip (along the direction indicated by the white arrow in Figure S8a), the junction was stretched and fractured at the outermost layer of the MWNT ("sword-in-sheath" failure) far away from the joint site (Figure S8b).[3] Therefore, the CNT-graphene junction exhibits better toughness than the CNT. The applied tensile force (F) at which the MWNT breaks can be estimated by the product of the tensile strength (σ_s) and cross-sectional area (S).[3] The measured tensile strength of a MWNT ranged from 11 to 63GPa, and we choose a medium value (35GPa) for our MWNTs prepared by arc discharge methods. By assuming that only the outermost shell of the tube carries the tensile load, and that the cross-sectional area of the outermost shell $S=\pi Dd$, where D is

the outer diameter of the nanotube (18nm for this MWNT) and *d* is the interlayer spacing of graphite, i.e. about 0.34 nm, the bonding force is therefore estimated to be at least ~670 nN.

Supplementary Movies

Movie S1: The structural evolution at atomic scale during a crystallization process of a SWNT/a-C/SWNT junction by molecular dynamics (MD) simulations

Reference

(1) K. Liew, X. Q. He, C. H. Wong, *Acta Mater.* 2004, **52**, 2521.

(2) J. Y. Huang, F. Ding, B. I. Yakobson, P. Lu, L. Qi, J. Li, *Proc. Nat. Acad.Sci*. 2009, **106**, 10103.

(3) M. F. Yu, O. Lourie, M. J. Dyer, K. Moloni, T. F. Kelly, R. S. Ruoff, Science 2000, **287**, 637.